Articles

Contribution from the Chemistry Department, University of Virginia, Charlottesville, Virginia 22901, and Physiology Department, School of Medicine, University of Virginia, Charlottesville, Virginia 22908

Comparison of Electric-Dipole Intensity Parameters for a Series of Structurally Related Neodymium, Holmium, and Erbium Complexes in Aqueous Solution. Theory and Experiment

Mark T. Devlin,[†] Eileen M. Stephens,*[‡] and F. S. Richardson[†]

Received October 8, 1987

Absorption intensity data are reported for multiplet-to-multiplet electronic transitions in a series of Nd(III), Ho(III), and Er(III) complexes in aqueous solution. These data are analyzed in terms of the Judd–Ofelt intensity parameters, Ω_λ (λ = 2, 4, 6), for 4f–4f electric-dipole transitions. Each of the complexes contains ligands that are terdentate under mildly alkaline solution conditions, and the terminal donor moieties in each ligand are carboxylate groups. The ligands differ only with respect to their central (middle) donor moieties and the geometries of their chelate rings (when coordinated to a metal ion). These small chemical and structural differences are shown to produce significant variations in the intensities of certain absorption bands, and their relative perturbations on 4f–4f transition intensities are readily apparent in the Ω_λ parameters determined for the various complexes. Theoretical calculations of Ω_λ parameters are reported for model structures of each complex. These calculations are based on a model that includes two different mechanisms for 4f–4f electric-dipole transition amplitudes, and the model structures adopted for the complexes each have tris(terdentate) coordination. Comparisons of calculated and empirically determined Ω_λ parameters suggest specific correlations between relative intensities, lanthanide–ligand–radiation interaction mechanisms, ligand structure (geometry, polarizability, and charge), and lanthanide ($4f^N$) electronic properties. Differential ligand effects are manifested most strongly in the Ω_2 intensity parameters, whereas lanthanide ion dependence is most apparent in the Ω_6 parameters.

Introduction

The 4f–4f absorption spectra of most lanthanide complexes in aqueous solution exhibit absorption bands that may be assigned to specific ground multiplet to excited multiplet transition manifolds. Each multiplet-to-multiplet transition manifold is generally comprised of a number of unresolved transitions between individual crystal field levels of the ground and excited multiplet states. If these transitions occur via a predominantly electric dipole mechanism *and* if all crystal field levels of the ground multiplet are assumed to be equally populated, the *total* (isotropic) oscillator strength of a multiplet-to-multiplet transition, $\psi J \rightarrow \psi' J'$, may be expressed as

$$f = (8\pi^2 m_e c/3h)\chi \bar{\nu}_{\psi' J'}(2J+1)^{-1}\sum_\lambda \Omega_\lambda \langle \psi J \| U^\lambda \| \psi' J' \rangle^2 \quad (1)$$

where λ = 2, 4, and 6, $\bar{\nu}_{\psi' J'}$ is the $\psi J \rightarrow \psi' J'$ transition energy (expressed in wavenumbers), χ is the Lorentz field correction for the refractivity of the sample medium, U^λ is an irreducible unit tensor operator (of rank λ), and the Ω_λ quantities are parameters that contain all the details of the lanthanide–ligand–radiation field (Ln–L–$h\nu$) interactions relevant to 4f–4f electric-dipole transition processes (in the one-electron–one-photon approximation). The U^λ matrix elements in eq 1 are evaluated over eigenstates of a $4f^N$ electronic Hamiltonian defined to be diagonal in a JM_J basis, and these matrix elements are independent of all nonspherically symmetric lanthanide–ligand (crystal field) interactions. Expression 1 is based on the Judd–Ofelt theory of 4f–4f electric-dipole intensity, and the Ω_λ parameters are generally called Judd–Ofelt intensity parameters.[1-5]

Oscillator strengths are defined in terms of experimental observables as

$$f = (4.32 \times 10^{-9})\int \epsilon(\bar{\nu})\, d\bar{\nu} \quad (2)$$

where ϵ is the molar (decadic) absorption coefficient, $\bar{\nu}$ is expressed in cm^{-1}, and the integration is over the transition region of interest. Expressions 1 and 2 may be combined to obtain

$$I(\psi' J') = (2.5 \times 10^{19})\chi \bar{\nu}_{\psi' J'}(2J+1)^{-1}\sum_\lambda \Omega_\lambda \langle \psi J \| U^\lambda \| \psi' J' \rangle^2 \quad (3)$$

where

$$I(\psi' J') = \int \epsilon(\bar{\nu})\, d\bar{\nu} \quad (4)$$

in which the integration is over the entire $\psi J \rightarrow \psi' J'$ absorption band, and the Ω_λ parameters are expressed in units of cm^2. Expression 3 provides the basis for analyzing empirical intensity data in terms of the Ω_λ intensity parameters. Values of $I(\psi' J')$ and $\bar{\nu}_{\psi' J'}$ are obtained from absorption measurements, the U^λ matrix elements are evaluated over the relevant $[SL]J$ state vectors, χ is assumed to have a fixed value (independent of $\bar{\nu}$), and the Ω_λ parameters are then adjusted to optimize fits between calculated and experimentally determined values of $I(\psi' J')$ for all $\psi J \rightarrow \psi' J'$ transitions accessible to measurement in the system of interest. The phenomenological intensity parameters obtained by this procedure provide a useful basis on which the 4f–4f intensity properties of different lanthanide systems may be compared, and their relative values may be used to develop useful spectra–structure relationships for various classes of lanthanide complexes.

Detailed interpretations of the Ω_λ parameters, and fully rationalized spectra–structure relationships based on these parameters, require explicit consideration of lanthanide and ligand structural properties (electronic and stereochemical) and Ln–L–$h\nu$ interaction mechanisms. Significant effort has been devoted to constructing theoretical models appropriate for calculating and rationalizing the Ω_λ intensity parameters in terms of specific structural properties and Ln–L–$h\nu$ interaction mechanisms. The greatest attention has been focused on the Ω_2 parameter, which exhibits by far the largest variations in magnitude among complexes with different ligand environments. The sensitivity of this parameter to the ligand environment explains the "hypersensitive" intensity behavior observed for certain $\psi J \rightarrow \psi' J'$ transitions.

[†] Chemistry Department.
[‡] Physiology Department.

(1) Judd, B. R. *Phys. Rev.* **1962**, *127*, 750.
(2) Ofelt, G. S. *J. Chem. Phys.* **1962**, *37*, 511.
(3) Axe, J. D. *J. Chem. Phys.* **1963**, *39*, 1154.
(4) Peacock, R. D. *Struct. Bonding (Berlin)* **1975**, *22*, 83.
(5) Carnall, W. T.; Beitz, J. V.; Crosswhite, H.; Rajnak, K.; Mann, J. B. In *Systematics and the Properties of the Lanthanides*; Sinha, S. P., Ed.; Reidel: Boston, 1983; pp 389–450.

0020-1669/88/1327-1517$01.50/0

These transitions exhibit extraordinarily large intensity variations among different complexes, and as a class, they follow the same ΔJ selection rules as the U^2 matrix elements in eq 3. It is expected, therefore, that their intensities will be modulated in large part by variations in the Ω_2 parameter.

In the present study, we examine the Ω_λ intensity parameters for six different complexes of Nd(III), Ho(III), and Er(III) formed in aqueous solution under mildly alkaline conditions. The ligands in these complexes are oxydiacetate (ODA), dipicolinate (DPA), chelidonate (CDO),[6] chelidamate (CDA),[7] iminodiacetate (IDA), and methyliminodiacetate (MIDA). Each of these complexes is expected to have predominantly tris(terdentate) coordination with trigonal symmetry (either D_3 or C_{3h}), and each has a $LnL_6L'_3$ coordination polyhedron in which the L donor atoms are located at the vertices of a trigonal prism (regular or slightly distorted) and the L' donor atoms occupy "capping" positions on normals to the rectangular faces of the prism. In each complex, the L donor atoms are carboxylate oxygens. The major structural differences between the complexes are found in (1) the nature of the L' donor atoms (or groups), (2) the spatial dispositions of the chelate rings, and (3) the constituent and substituent atoms and bonds of the chelate rings. These complexes are particularly well-suited for investigating *quantitatively* the ligand dependence of the Ω_λ intensity parameters. They have well-defined structural differences with respect to both geometry and chemical makeup, and they are amenable to study by several theoretical models that have been proposed for 4f–4f electric-dipole intensity. Furthermore, Nd(III), Ho(III), and Er(III) each exhibit at least one "hypersensitive" $\psi J \rightarrow \psi' J'$ transition in the near-ultraviolet–visible region of the spectrum,[4,8] and possible lanthanide "size" effects should be apparent from comparisons of results obtained for Nd(III) (which is relatively large) and for Ho(III) and Er(III) (which are smaller than Nd(III)).

In two previous papers,[9,10] we reported experimental results and model calculations on the 4f–4f intensity properties of Nd(III) and Ho(III) complexes with ODA, DPA, IDA, and MIDA in aqueous solution. In the present paper, we report *new* experimental and theoretical results for these systems *and* for Nd(III) and Ho(III) complexes with the CDO and CDA ligands. Most of the Er(III) results cited in the present paper were taken directly from two previously published reports.[11,12] The only exceptions are found in the theoretical results for several model structures, which were altered slightly from those considered previously.

The main emphasis in this paper is on *comparisons* of Ω_λ parameters obtained for (1) complexes containing different ligands but the same lanthanide and (2) complexes containing different lanthanides but the same ligand. These comparisons are made for Ω_λ values derived from empirical intensity data according to eq 3 *and* for Ω_λ values calculated according to a specific theoretical model for 4f–4f electric-dipole intensity. The theoretically calculated results help rationalize and explain the differences and trends observed among the Ω_λ parameters determined for the various complexes examined in this study. In most cases, these differences and trends can be related to specific structural features in the ligand environment.

The intensity model employed in the present study is identical with that described in several previous papers from our laboratory,[13,14] and the strategies used in parametrizing this model in terms of ligand structural properties have also been described previously.[10,12,15-17] Two different Ln–L–$h\nu$ interaction mechanisms are incorporated in this model, and our results indicate that "interferences" between these two mechanisms can make significant contributions to the Ω_λ parameters. This model requires further calibration to achieve quantitative predictive power. However, in its applications to date it has generally produced results in good qualitative and semiquantitative agreement with experiment.

Table I. Transition Regions and Intraconfigurational U^λ Reduced Matrix Elements Used in the Intensity Analyses

transition regions[a]			$\langle\|U^\lambda\|\rangle^2/10^{-3}$		
label	excited multiplets	approx $\bar{\nu}_{max}$/cm^{-1}	$\lambda = 2$	$\lambda = 4$	$\lambda = 6$
Nd(a)	$^4F_{3/2}$	11 600	0.00	229	56.0
Nd(b)	$^4F_{5/2}$, $^2H_{9/2}$	12 500	10.0	241	517
Nd(c)	$^4F_{7/2}$, $^4S_{3/2}$	13 400	1.15	43.2	661
Nd(d)	$^4F_{9/2}$	14 700	0.92	9.31	40.4
Nd(e)	$^4G_{5/2}$, $^2G_{7/2}$	17 200	972	595	64.4
Nd(f)	$^4G_{7/2}$, $^4G_{9/2}$, $^2K_{13/2}$	19 000	67.5	221	126
Nd(g)	$^2G_{9/2}$, $^2D_{3/2}$, $^4G_{11/2}$, $^2K_{15/2}$	21 300	1.03	46.4	36.8
Nd(h)	$^2P_{1/2}$, $^2D_{5/2}$	23 300	0.00	41.1	1.77
Nd(i)	$^4D_{3/2}$, $^4D_{5/2}$, $^4D_{1/2}$, $^2I_{11/2}$	28 000	4.95	523	48.4
Nd(j)	$^2L_{15/2}$, $^4D_{7/2}$, $^2I_{13/2}$	30 400	0.14	30.2	19.8
Ho(a)	$^5F_5$	15 600	0.00	423	571
Ho(b)	$^5S_2$, $^5F_4$	18 600	0.00	240	923
Ho(c)	$^5F_3$, $^5F_2$, $^3K_8$	20 900	20.5	31.7	704
Ho(d)	$^5G_6$, $^5F_1$	22 200	1500	829	140
Ho(e)	$^5G_5$	24 000	0.00	529	0.01
Ho(f)	$^5G_4$, $^3K_7$	25 900	5.72	38.5	68.2
Ho(g)	$^5G_5$, $^3H_6$, $^5F_2$	27 600	238	218	166
Ho(h)	$^5G_3$, $^3L_9$	28 900	17.9	5.17	163
Ho(i)	$^3F_4$, $^3K_6$, $^5G_2$	29 900	2.81	126	8.03

[a] All Nd transitions originate from the $^4I_{9/2}$ ground multiplet, and all Ho transitions originate from the $^5I_8$ ground multiplet. Excited multiplets are labeled according to their major *SLJ* components. Note that most of the transition regions span more than one excited multiplet manifold.

Experimental Section

$NdCl_3 \cdot 6H_2O$ (99.9%) and $HoCl_3 \cdot 6H_2O$ (99.99%) were purchased from Aesar and were used without further purification. Oxydiacetic acid, methyliminodiacetic acid, chelidonic acid hydrate, and dipicolinic acid were purchased from Aldrich and used without further purification. Chelidamic acid hydrate was purchased from Aldrich and was purified twice, by using the procedure described by Bag et al.[18] Iminodiacetic acid was purchased from Sigma and used without further purification.

All spectroscopic measurements were carried out on aqueous solution samples in which $[Ho^{3+}]$ or $[Nd^{3+}] = 10$ mM. For $NdCl_3$ and for $HoCl_3$ in solution, the pH was approximately 4. A 1:3 concentration ratio of lanthanide to ligand was used in each of the ligand studies, with a solution pH between 7.5 and 8.2. Solution pH adjustments were made with NH_4OH. Absorption spectra were recorded at room temperature on a Kontron UVIKON 860 spectrophotometer and stored in digital form.

Absorption spectra were obtained over the 11 500–30 500-cm^{-1} energy region for the Nd(III) complexes. This region contains 24 multiplet-to-multiplet transitions that originate from the $^4I_{9/2}$ ground multiplet of Nd(III). However, the absorption spectra exhibit only 10 resolved bands, eight of which are composites of several multiplet-to-multiplet transition manifolds (see Table I). Absorption spectra for the Ho(III) complexes were obtained over the 15 500–30 500-cm^{-1} energy region. This region contains 19 multiplet-to-multiplet transitions that originate from the $^5I_8$ ground multiplet of Ho(III), but the absorption spectra exhibit only nine resolved bands. Seven of these bands are composites of several multiplet-to-multiplet transition manifolds (see Table I). Integrated band intensities were determined for each of the transition regions listed in

(6) Chelidonate (CDO) refers here to the deprotonated form of chelidonic acid (4-hydroxypyran-2,6-dicarboxylic acid) in aqueous solution under alkaline pH conditions.
(7) Chelidamate (CDA) refers here to the deprotonated form of chelidamic acid (4-hydroxypyridine-2,6-dicarboxylic acid) in aqueous solution under alkaline pH conditions.
(8) Henrie, D. E.; Fellows, R. L.; Choppin, G. R. *Coord. Chem. Rev.* **1976**, *18*, 199.
(9) Stephens, E. M.; Davis, S. A.; Reid, M. F.; Richardson, F. S. *Inorg. Chem.* **1984**, *23*, 4607.
(10) Stephens, E. M.; Reid, M. F.; Richardson, F. S. *Inorg. Chem.* **1984**, *23*, 4611.
(11) Devlin, M. T.; Stephens, E. M.; Richardson, F. S.; Van Cott, T. C.; Davis, S. A. *Inorg. Chem.* **1987**, *26*, 1204.
(12) Devlin, M. T.; Stephens, E. M.; Richardson, F. S. *Inorg. Chem.* **1987**, *26*, 1208.
(13) Reid, M. F.; Richardson, F. S. *J. Chem. Phys.* **1983**, *79*, 5735.
(14) Reid, M. F.; Richardson, F. S. *J. Phys. Chem.* **1984**, *88*, 3579.
(15) Richardson, F. S.; Saxe, J. D.; Davis, S. A.; Faulkner, T. R. *Mol. Phys.* **1981**, *42*, 1401.
(16) Saxe, J. D.; Faulkner, T. R.; Richardson, F. S. *J. Chem. Phys.* **1982**, *76*, 1607.
(17) Dallara, J. J.; Reid, M. F.; Richardson, F. S. *J. Phys. Chem.* **1984**, *88*, 3587.
(18) Bag, S. P.; Fernando, Q.; Freiser, H. *Inorg. Chem.* **1962**, *1*, 887.

Table I, and the total oscillator strength for each of these regions was calculated according to eq 2.

Empirical Intensity Parameters

Experimentally determined oscillator strengths for each system were fitted to eq 1 by a linear least-squares fitting procedure in which the Ω_λ parameters are treated as free variables. A fixed value of 1.19 was assigned to χ, and the transition energy for each transition region was obtained from the approximate baricenter location of the relevant absorption band. The values used for the U^λ reduced matrix elements (*squared*) are listed in Table I. The $\langle\|U^\lambda\|\rangle^2$ values listed for *composite* transition regions are actually sums over the $\langle\psi J\|U^\lambda\|\psi' J'\rangle^2$ values computed for the $\psi J \rightarrow \psi' J'$ component transitions.

The Ω_λ parameters obtained from these intensity data fits are referred to, hereafter, as *empirical intensity parameters*, and the oscillator strengths calculated from eq 1 by using these empirical intensity parameters are referred to as *fitted* oscillator strengths. Among the 14 empirical data sets analyzed in this study (seven for neodymium complexes and seven for holmium complexes), 10 contain nine data points, two contain seven data points, and two contain six data points (vide infra).

Theory

Intensity Model. In our theoretical considerations of 4f–4f (multiplet-to-multiplet) transition intensities, we assume the general validity of eq 1. Our main objective is to rationalize the Ω_λ parameters in terms of specific Ln–L–*hν* interaction mechanisms and structural properties of the lanthanide complexes. In this study, we consider two mechanisms for 4f–4f electric-dipole intensities. These mechanisms are commonly referred to as the *static-coupling* (or static-charge) and *dynamic-coupling* (or ligand-polarization) mechanisms.[13,14] Intensity contributions requiring lanthanide–ligand orbital overlap and vibronic interactions are ignored in our applications of these mechanisms.

In examining the static-coupling (SC) and dynamic-coupling (DC) mechanistic contributions to 4f–4f electric-dipole intensity, it is useful to express the Ω_λ parameters in terms of another set of parameters:

$$\Omega_\lambda = (2\lambda + 1)^{-1}\sum_{t,p}|A^\lambda_{tp}|^2 \tag{5}$$

where the A^λ_{tp} parameters are defined to parametrize the electric-dipole transition moments associated with transitions between individual crystal field (Stark) levels.[13,14] Each A^λ_{tp} parameter may be partitioned into separate mechanistic contributions, and in the present study, we may write

$$A^\lambda_{tp} = A^\lambda_{tp}[\mathrm{SC}] + A^\lambda_{tp}[\mathrm{DC}] \tag{6}$$

Substituting eq 6 into eq 5, we obtain

$$\Omega_\lambda = \Omega_\lambda[\mathrm{SC}] + \Omega_\lambda[\mathrm{DC}] + \Omega_\lambda[\mathrm{SC,DC}] \tag{7}$$

where

$$\Omega_\lambda[\mathrm{SC}] = (2\lambda + 1)^{-1}\sum_{t,p}|A^\lambda_{tp}[\mathrm{SC}]|^2 \tag{8}$$

$$\Omega_\lambda[\mathrm{DC}] = (2\lambda + 1)^{-1}\sum_{t,p}|A^\lambda_{tp}[\mathrm{DC}]|^2 \tag{9}$$

$$\Omega_\lambda[\mathrm{SC,DC}] = (2\lambda + 1)^{-1} \times \sum_{t,p}(A^\lambda_{tp}[\mathrm{SC}]\, A^{\lambda *}_{tp}[\mathrm{DC}] + A^{\lambda *}_{tp}[\mathrm{SC}]\, A^\lambda_{tp}[\mathrm{DC}]) \tag{10}$$

and asterisks denote complex conjugation. The $\Omega_\lambda[\mathrm{SC}]$ parameters are derived entirely from the static-coupling mechanism, the $\Omega_\lambda[\mathrm{DC}]$ parameters are derived entirely from the dynamic-coupling mechanism, and the $\Omega_\lambda[\mathrm{SC,DC}]$ parameters are derived from interferences between transition moments induced by the SC and DC mechanisms.[13,14] The $\Omega_\lambda[\mathrm{SC}]$ and $\Omega_\lambda[\mathrm{DC}]$ parameters are, of course, always positive in sign, whereas the $\Omega_\lambda[\mathrm{SC,DC}]$ parameters may be either positive or negative in sign, depending on the relative phases of the SC and DC electric-dipole transition moments.

Details of the A^λ_{tp} parametrization scheme for 4f–4f electric-dipole transition moments, descriptions of the static- and dynamic-coupling mechanisms, and explicit expressions for the $A^\lambda_{tp}[\mathrm{SC}]$ and $A^\lambda_{tp}[\mathrm{DC}]$ terms of eq 6 have been given in previous papers.[10,12–14,17] These details will not be repeated here. In general, our intensity model assumes that the ligand environment can be represented as an array of atomic and chemical-bond perturber sites, each with a characteristic electric charge and/or polarizability, and each site is presumed to perturb the $4f^N$ electronic configuration of the lanthanide via purely electrostatic interactions. Each *atomic* perturber site is assigned a net charge and an isotropic polarizability, and each *chemical-bond* perturber site is characterized by an anisotropic polarizability, which is assumed to be cylindrically symmetric about the bond axis. The $A^\lambda_{tp}[\mathrm{SC}]$ parameters depend on perturber site charges (eq_L) and positional coordinates (R_L, θ_L, ϕ_L) *and* on a set of electronic parameters characteristic of the lanthanide ion (vide infra). The $A^\lambda_{tp}[\mathrm{DC}]$ parameters depend on perturber site polarizabilities and positional coordinates and on the radial expectation values $\langle r^\lambda\rangle$ of the 4f electrons. For chemical-bond perturber sites, the polarizabilities are characterized in terms of two components, one parallel and one perpendicular to the bond axis, and the orientation of each bond with respect to a fixed coordinate system in the complex also enters into the expression for $A^\lambda_{tp}[\mathrm{DC}]$.[13,14,17]

In our model, the static- and dynamic-coupling mechanisms make independent contributions to the A^λ_{tp} parameters (see eq 6) and each ligand perturber site makes a separate (and independent) contribution to the $A^\lambda_{tp}[\mathrm{SC}]$ and/or $A^\lambda_{tp}[\mathrm{DC}]$ parameters. However, the Ω_λ parameters, as defined by eq 5, will contain contributions with *mixed* mechanistic origins (see eq 7 and 10), and they will include terms dependent on the properties of *pairs* of ligand perturber sites.

Calculations. The $A^\lambda_{tp}[\mathrm{SC}]$ and $A^\lambda_{tp}[\mathrm{DC}]$ parameters were calculated in the present study according to the expressions

$$A^\lambda_{tp}[\mathrm{SC}] = N^\lambda_t[\mathrm{SC}]\; e^2\Xi(t,\lambda)\; (-1)^p\sum_\mathrm{L} q_\mathrm{L}\; \mathbf{C}^t_{-p}(\theta_\mathrm{L},\phi_\mathrm{L})\; R_\mathrm{L}^{-(t+1)} \tag{11}$$

$$A^\lambda_{tp}[\mathrm{DC},\bar{\alpha}] = N^\lambda_t[\mathrm{DC},\bar{\alpha}]\; \langle r^\lambda\rangle(-1)^p\sum_\mathrm{L}\bar{\alpha}_\mathrm{L}\; \mathbf{C}^t_{-p}(\theta_\mathrm{L},\phi_\mathrm{L})\; R_\mathrm{L}^{-(\lambda+2)} \tag{12}$$

$$A^\lambda_{tp}[\mathrm{DC},\beta] = N^\lambda_t[\mathrm{DC},\beta] \times \langle r^\lambda\rangle(-1)^p\sum_\mathrm{L}\beta_\mathrm{L}\{\mathbf{C}^{\lambda+1}(\theta_\mathrm{L},\phi_\mathrm{L})\; \mathbf{C}^2(\theta_\mathrm{L}',\phi_\mathrm{L}')\}^t_{-p}R_\mathrm{L}^{-(\lambda+2)} \tag{13}$$

where

$$A^\lambda_{tp}[\mathrm{DC}] = A^\lambda_{tp}[\mathrm{DC},\bar{\alpha}] + A^\lambda_{tp}[\mathrm{DC},\beta]$$

$$N^\lambda_t[\mathrm{SC}] = (2\lambda + 1)(2t + 1)^{-1/2}\delta_{t,\lambda\pm1}$$

$$N^\lambda_t[\mathrm{DC},\bar{\alpha}] = 7\begin{pmatrix} 3 & \lambda & 3 \\ 0 & 0 & 0 \end{pmatrix}[t(2\lambda + 1)]^{1/2}\delta_{t,\lambda+1}$$

$$N^\lambda_t[\mathrm{DC},\beta] = -7(10/3)^{1/2}\begin{pmatrix} 3 & \lambda & 3 \\ 0 & 0 & 0 \end{pmatrix}\begin{Bmatrix} \lambda & \lambda+1 & 1 \\ 2 & 1 & t \end{Bmatrix} \times [(\lambda + 1)(2\lambda + 1)(2\lambda + 3)]^{1/2}$$

The polarizability quantities, $\bar{\alpha}_\mathrm{L}$ and β_L, appearing in eq 12 and 13 are defined as follows: $\bar{\alpha}_\mathrm{L} = {}^1/_3(\alpha_\mathrm{L}^\parallel + 2\alpha_\mathrm{L}^\perp)$ and $\beta_\mathrm{L} = \alpha_\mathrm{L}^\parallel - \alpha_\mathrm{L}^\perp$, where $\alpha_\mathrm{L}^\parallel$ and $\alpha_\mathrm{L}^\perp$ denote polarizability components defined parallel ($\parallel$) and perpendicular ($\perp$) to the cylindrically symmetric axis of perturber group L. In our treatment, the only contributions to $A^\lambda_{tp}[\mathrm{DC},\beta]$ are from chemical bonds and the only contributions to $A^\lambda_{tp}[\mathrm{SC}]$ are from atomic perturber sites. Both atoms *and* bonds contribute to $A^\lambda_{tp}[\mathrm{DC},\bar{\alpha}]$. The spherical tensor $\mathbf{C}^2_m(\theta_\mathrm{L}',\phi_\mathrm{L}')$ in expression 13 rotates the bond axis of L to an orientation parallel to the Z axis of the coordinate system adopted for the overall complex. For chemical bonds, the (R_L, θ_L, ϕ_L) coordinates locate the bond *midpoints*. The $\Xi(t,\lambda)$ quantity in eq 11 depends entirely on the electronic properties of the lanthanide ion, and it is defined here exactly as in eq 14 of Judd.[1]

Lanthanide Electronic Parameters. The lanthanide electronic parameters required to evaluate eq 11–13 are $\Xi(t,\lambda)$ and $\langle r^\lambda\rangle$. Values for the $\Xi(t,\lambda)$ parameters were taken from a study by Leavitt and Morrison,[19] and values for the $\langle r^\lambda\rangle$ parameters were

(19) Leavitt, R. P.; Morrison, C. A. *J. Chem. Phys.* **1980**, *73*, 749.

taken from a study by Morrison and Leavitt.[20] These values of $\Xi(t,\lambda)$ and $\langle r^\lambda \rangle$ are listed in Table II.

Model Structures and Ligand Parameters. Calculations were carried out for model structures of the six tris(terdentate) complexes $Ln(ODA)_3^{3-}$, $Ln(DPA)_3^{3-}$, $Ln(CDO)_3^{6-}$, $Ln(CDA)_3^{6-}$, $Ln(IDA)_3^{3-}$, and $Ln(MIDA)_3^{3-}$. The Ln(ODA), Ln(DPA), Ln(CDO), and Ln(CDA) structures each have D_3 symmetry, and the Ln(IDA) and Ln(MIDA) structures each have C_{3h} symmetry. Detailed descriptions of these structures and the rationale for using them in model calculations have been presented previously.[10,12] The geometries adopted for these structures in the present study are identical with those used in our previously reported calculations on Nd(III), Ho(III), and Er(III) complexes.[10,12] The distribution of perturber sites and the assignments of perturber charge (q_L) and polarizability ($\bar{\alpha}_L$, β_L) parameters are also identical with those described in ref 12 *except* for the Ln(CDO) structure. For the Ln(CDO) structure, new polarizability parameters were assigned to the oxygen atom and the two carbon–oxygen bonds within the pyran ring. The new (and old) parameters are as follows: pyran oxygen atom, $\bar{\alpha} = 0.47$ Å^3 (0.21 Å^3); pyran carbon–oxygen bonds, $\bar{\alpha} = 0.68$ Å^3 (0.60 Å^3) and $\beta = -0.50$ Å^3 (0.43 Å^3). The old parameters are essentially identical with those used for the Ln(ODA) structure, and the new parameters were chosen to reflect pyran ring unsaturation (and π-electron contributions to polarizability).

Calculations were also carried out for model structures of the aquo complexes $Ln(H_2O)_9^{3+}$ and $Ln(H_2O)_8^{3+}$. In each structure, the water molecules are represented as single perturber sites with the oxygen atoms assigned an effective charge of −0.3e and an isotropic polarizability of 1.49 Å^3. The nine-coordinate structure has D_{3h} symmetry with the water oxygen atoms forming a *tricapped-trigonal-prism* polyhedron. The eight-coordinate structure has D_{4d} symmetry with the oxygen atoms forming a *square-antiprism* polyhedron. The Ln–O bond lengths were assumed to be 2.5 Å.

The model structures used in our intensity calculations were designed to mimic the *majority* species formed in aqueous solution by the various lanthanide–ligand systems examined in this study. These structures are idealized models of the most probable "real" complexes, and the properties assigned to the various structures are those most likely to influence 4f–4f electric-dipole transition intensities. These properties may or may not be important to the relative binding strengths of the various complexes. The binding strengths of lanthanide complexes are generally presumed to be nearly independent of 4f-electron–ligand interactions, whereas 4f–4f electric-dipole intensities have *essential* dependence on these interactions.

The individual chelate rings in four of our model tris(terdentate) structures are

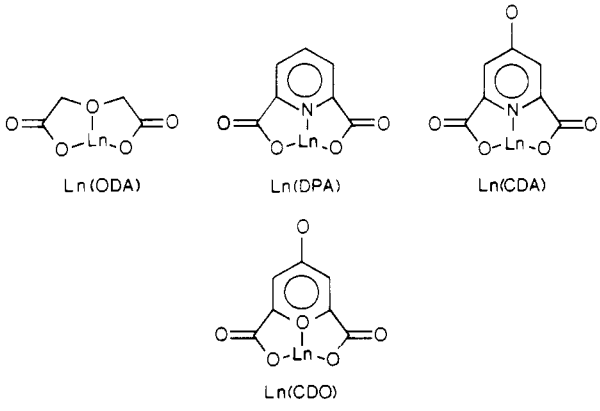

In each case the chelate ring is planar, and in the tris complexes these chelate rings stretch diagonally across the rectangular faces of a tricapped trigonal prism formed by the coordinated (donor) atoms of the ligands. The tris complexes have D_3 symmetry, and in our model structures each $LnL_6L'_3$ coordination polyhedron also has D_3 symmetry. In our intensity calculations, these structures are differentiated only by the charge and polarizability properties assigned to the respective L′ atoms and their substituent moieties.

The chelate rings in the Ln(IDA) and Ln(MIDA) model structures are *not* planar, and the ligands are wrapped around the $LnL_6L'_3$ coordination polyhedron (a tricapped trigonal prism) in a *facial* configuration.[21,22] These structures each have C_{3h} symmetry, and they are differentiated only by the H vs CH_3 substituent on the nitrogen (imino) donor atoms.

Table II. Lanthanide Electronic Parameters Used To Calculate Theoretical Intensity Parameters

parameter	Nd(III)	Ho(III)	Er(III)
$\Xi(1,2)/10^{-6}$ cm^2 erg^{-1}	−1.24	−0.971	−0.961
$\Xi(3,2)/10^{-22}$ cm^4 erg^{-1}	1.56	0.893	0.874
$\Xi(3,4)/10^{-22}$ cm^4 erg^{-1}	1.40	0.901	0.884
$\Xi(5,4)/10^{-38}$ cm^6 erg^{-1}	−3.90	−1.10	−1.14
$\Xi(5.6)/10^{-38}$ cm^6 erg^{-1}	−4.27	−2.49	−2.43
$\Xi(7,6)/10^{-54}$ cm^8 erg^{-1}	6.83	3.34	3.16
$\langle r^2 \rangle/10^{-17}$ cm^2	1.706	1.692	1.706
$\langle r^4 \rangle/10^{-33}$ cm^4	5.776	4.217	4.126
$\langle r^6 \rangle/10^{-48}$ cm^6	1.590	1.012	0.983

Results

Experimental and fitted oscillator strengths are listed in Tables III and IV for each of the Nd(III) and Ho(III) complexes examined in this study. Among the neodymium absorption bands, the one labeled as Nd(e) exhibits the greatest variations in intensity. The Nd(b), Nd(c), and Nd(f) bands also exhibit significant intensity variations, but much less so than the Nd(e) band. Among the holmium absorption bands, the one labeled as Ho(d) exhibits by far the greatest intensity variations, but the Ho(g) band also shows significant variations in intensity. From Tables III and IV we note that oscillator strengths were not determined for several transition regions of the CDO and CDA complexes. This was due to the onset of a broad and very intense ligand absorption band, which in large part masks the 4f → 4f transitions in these regions.

The Ω_λ parameters obtained from intensity data fits are listed in Table V. The relatively large uncertainties in the parameters obtained for Nd(CDO) and Nd(CDA) reflect the smallness of the empirical data sets available for these systems (see Table III). We have previously reported Ω_λ parameters for the ODA, DPA, IDA, and MIDA complexes of both Nd(III) and Ho(III).[9] However, the number of absorption bands included in our previous study was less than the number considered here for each system, and the results presented in Table V should be considered more reliable and accurate than those reported in ref 9. Ratios of Ω_λ(complex) vs Ω_λ(aquo) are given in Table VI, and comparisons of the empirical intensity parameters determined for the Nd(III) complexes vs those for the Ho(III) and Er(III) complexes are given in Table VII.

Intensity parameters calculated for model structures of Nd(III) and Ho(III) complexes are listed in Tables VIII and IX. The Ω_2 parameter vanishes by symmetry for the eight-coordinate $Ln(H_2O)_8$ model structures. These structures have D_{4d} symmetry, and all the A^2_{tp} parameters have values of 0 in this symmetry. For each of the other structures, the Ω_2 parameter is dominated by contributions from the dynamic-coupling mechanism. The dynamic-coupling mechanism also makes the dominant contributions to the Ω_4 and Ω_6 parameters calculated for the $Ln(H_2O)_8$ and $Ln(H_2O)_9$ structures. However, for each of the other structures, the static- *and* dynamic-coupling mechanisms make comparable contributions to Ω_4, and the Ω_6 parameter is overwhelmingly dominated by contributions from the static-coupling mechanism. We also note that the [SC,DC] terms make important contributions to the Ω_2 and Ω_4 parameters calculated for

(20) Morrison, C. A.; Leavitt, R. P. *J. Chem. Phys.* **1979**, *71*, 2366.

(21) Favas, M. C.; Kepert, D. L. *Prog. Inorg. Chem.* **1981**, *28*, 309.
(22) Foster, D. R.; Richardson, F. S. *Inorg. Chem.* **1983**, *22*, 3996.

Table III. Experimental and Fitted Oscillator Strengths for Nd(III) Complexes[a]

transition region[b]	complexes							
	aquo		ODA		DPA		CDO	
	exptl	fit	exptl	fit	exptl	fit	exptl	fit
Nd(a)	nd[c]	nd	nd	nd	nd	nd	2.16	2.90
Nd(b)	7.97	7.64	9.21	8.83	11.99	11.53	10.80	11.85
Nd(c)	7.97	8.32	9.80	10.27	12.79	13.54	14.47	13.45
Nd(d)	0.53	0.62	0.64	0.74	0.86	0.97	0.97	0.99
Nd(e)	9.08	9.08	11.68	11.77	18.15	18.32	26.36	26.53
Nd(f)	6.17	4.83	6.63	5.28	9.73	7.02	11.85	7.97
Nd(g)	1.83	1.29	1.78	1.39	2.48	1.79	nd	nd
Nd(h)	0.24	0.61	0.28	0.54	0.42	0.66	nd	nd
Nd(i)	8.99	9.92	8.11	9.16	9.31	11.33	nd	nd
Nd(j)	2.36	1.09	1.81	1.14	2.25	1.46	nd	nd

transition region[b]	complexes					
	CDA		IDA		MIDA	
	exptl	fit	exptl	fit	exptl	fit
Nd(a)	2.34	3.50	nd	nd	nd	nd
Nd(b)	12.44	13.31	10.50	9.91	9.46	8.93
Nd(c)	15.65	14.78	10.52	11.21	9.46	10.07
Nd(d)	0.86	1.09	0.78	0.82	0.64	0.74
Nd(e)	26.25	26.55	15.28	15.39	14.50	14.59
Nd(f)	13.35	8.91	7.99	6.31	7.14	5.76
Nd(g)	nd	nd	2.13	1.62	1.86	1.46
Nd(h)	nd	nd	0.32	0.69	0.37	0.62
Nd(i)	nd	nd	10.12	11.52	9.26	10.47
Nd(j)	nd	nd	2.13	1.34	1.94	1.21

[a] Values given as $f/10^{-6}$. [b] See Table I. [c] Values not determined.

Table IV. Experimental and Fitted Oscillator Strengths for Ho(III) Complexes[a]

transition region[b]	complexes							
	aquo		ODA		DPA		CDO	
	exptl	fit	exptl	fit	exptl	fit	exptl	fit
Ho(a)	3.62	3.66	4.90	4.91	5.06	4.83	6.16	5.92
Ho(b)	5.40	5.00	7.33	6.96	7.16	6.79	8.57	8.17
Ho(c)	2.97	3.47	4.53	5.07	4.15	5.01	5.02	6.06
Ho(d)	5.91	5.91	16.50	16.53	22.80	22.90	36.56	36.64
Ho(e)	3.03	3.18	3.69	3.91	3.37	3.92	4.36	5.03
Ho(f)	1.02	0.65	1.03	0.93	0.92	0.94	1.11	1.18
Ho(g)	2.92	2.67	5.99	5.32	7.95	6.54	11.13	9.71
Ho(h)	0.68	1.11	1.11	1.73	1.10	1.78	nd[c]	nd
Ho(i)	0.76	1.00	0.87	1.27	0.77	1.29	nd	nd

transition region[b]	complexes					
	CDA		IDA		MIDA	
	exptl	fit	exptl	fit	exptl	fit
Ho(a)	6.06	5.83	5.37	5.37	3.97	4.15
Ho(b)	8.39	8.06	7.80	7.22	6.10	5.65
Ho(c)	4.95	5.96	4.30	5.06	3.60	4.05
Ho(d)	33.88	34.02	18.45	18.45	17.89	17.88
Ho(e)	4.25	4.93	4.61	4.88	3.64	3.65
Ho(f)	1.23	1.15	0.95	1.00	0.88	0.79
Ho(g)	10.93	9.15	6.18	5.86	5.54	5.25
Ho(h)	nd	nd	0.95	1.73	1.02	1.42
Ho(i)	nd	nd	1.10	1.56	0.86	1.18

[a] Values given as $f/10^{-6}$. [b] See Table I. [c] Values not determined.

most of the model structures, and these contributions are *subtractive* for Ω_4.

Ratios of the calculated vs empirically determined Ω_λ parameters are given in Table X, and in Table XI we list *relative* Ω_λ values using the Ln(ODA) complex as a reference system. The Nd and Ho results are from data presented in Tables V, VIII, and IX of the present paper, and the Er results are from ref 12 *except* for the Er(CDO) system. New calculations were carried out for Er(CDO) incorporating the revised ligand polarizability parameters described earlier (vide supra). The results given in Table X show that our model calculations generally overestimate the values of the Ω_2 parameters and underestimate the values of Ω_4 and Ω_6. The largest discrepancies between theory and experiment occur for the Ln(IDA) and Ln(MIDA) complexes, and the Nd calculations generally produced results in less good agreement with experiment than the Ho and Er calculations.

The Ω_λ parameters calculated and experimentally determined for Ln(aquo) complexes are summarized in Table XII. Attempts to fit experimental intensity data with only two parameters, Ω_4 and Ω_6, were unsuccessful. The empirically determined value of Ω_2 for Er(aquo) appears to be anomalously high, but it is close to the value (15.9×10^{-21} cm^2) reported by Carnall et al.[23] for Er^{3+} in dilute $HClO_4$ solution.

Discussion

Empirical Intensity Parameters. Considering the Ln(aquo) complexes as reference systems, and examining the results given in Tables V and VI, we note the following: (1) the Ω_2 parameters

(23) Carnall, W. T.; Fields, P. R.; Rajnak, K. *J. Chem. Phys.* **1968**, *49*, 4412.

Table V. Intensity Parameters Obtained from Data Fits[a]

system[b]	$\Omega_\lambda/10^{-21}$ cm^2		
	$\lambda = 2$	$\lambda = 4$	$\lambda = 6$
Nd(aquo)	9.0 ± 4.7	45.6 ± 5.6	68.8 ± 4.0
Nd(ODA)	24.2 ± 4.5	39.2 ± 5.5	85.6 ± 3.9
Nd(DPA)	47.0 ± 9.8	47.8 ± 11.7	113.1 ± 8.3
Nd(CDO)	79.5 ± 22.8	56.2 ± 33.3	112.3 ± 14.7
Nd(CDA)	69.9 ± 26.0	70.9 ± 38.0	122.8 ± 16.8
Nd(IDA)	33.1 ± 6.0	50.8 ± 7.2	93.0 ± 5.1
Nd(MIDA)	32.9 ± 5.1	46.2 ± 6.2	83.6 ± 4.4
Ho(aquo)	2.4 ± 2.3	32.7 ± 3.4	29.5 ± 1.9
Ho(ODA)	38.8 ± 2.8	40.2 ± 4.1	42.4 ± 2.3
Ho(DPA)	63.9 ± 4.5	40.3 ± 6.7	41.1 ± 3.7
Ho(CDO)	110.9 ± 5.7	51.7 ± 8.6	48.6 ± 4.8
Ho(CDA)	101.1 ± 6.2	50.7 ± 9.3	48.1 ± 5.2
Ho(IDA)	40.9 ± 3.4	50.1 ± 5.0	41.8 ± 2.8
Ho(MIDA)	46.4 ± 2.3	37.6 ± 3.4	33.2 ± 1.9

[a] All values are given to within $\pm 1\sigma$ as determined from the data-fitting procedure described in the text. [b] Nd(aq) and Ho(aq) refer respectively to $NdCl_3$ and $HoCl_3$ dissolved in water. All other systems refer to aqueous solutions with 1:3 lanthanide-to-ligand concentration ratios and solution pH between 7 and 9.

Table VI. Ratios of Empirical Intensity Parameters[a,b]

complex	Ω_λ(complex)/Ω_λ(aquo)		
	$\lambda = 2$	$\lambda = 4$	$\lambda = 6$
Nd(ODA)	2.69	0.86	1.24
Nd(DPA)	5.22	1.05	1.64
Nd(CDO)	8.83	1.23	1.63
Nd(CDA)	7.77	1.55	1.78
Nd(IDA)	3.68	1.11	1.35
Nd(MIDA)	3.66	1.01	1.22
Ho(ODA)	16.2	1.23	1.44
Ho(DPA)	26.6	1.23	1.39
Ho(CDO)	46.2	1.58	1.65
Ho(CDA)	42.1	1.55	1.63
Ho(IDA)	17.0	1.53	1.42
Ho(MIDA)	19.3	1.15	1.13
Er(ODA)	2.59	0.85	1.51
Er(DPA)	3.85	0.88	1.51
Er(CDO)	5.15	1.08	1.59
Er(CDA)	5.93	1.34	1.66
Er(IDA)	2.63	1.14	1.14
Er(MIDA)	3.55	1.05	1.35

[a] The Nd and Ho data are from Table V of the present paper. [b] The Er data are from Table V of ref 11. For Er(aquo): $\Omega_2 = 20.3 \times 10^{-21}$ cm^2, $\Omega_4 = 19.0 \times 10^{-21}$ cm^2, and $\Omega_6 = 21.4 \times 10^{-21}$ cm^2.

Table VII. Comparisons of Empirical Intensity Parameters for Nd(III), Ho(III), and Er(III) Complexes[a]

complex	Ω_λ(Nd)/Ω_λ(Ho)			Ω_λ(Nd)/Ω_λ(Er)		
	$\lambda = 2$	$\lambda = 4$	$\lambda = 6$	$\lambda = 2$	$\lambda = 4$	$\lambda = 6$
Ln(aquo)	3.75	1.39	2.33	0.44	2.40	3.21
Ln(ODA)	0.63	0.99	2.02	0.46	2.43	2.65
Ln(DPA)	0.74	1.19	2.75	0.60	2.86	3.50
Ln(CDO)	0.72	1.09	2.31	0.66	2.73	3.29
Ln(CDA)	0.69	1.40	2.55	0.59	2.78	3.45
Ln(IDA)	0.80	1.01	2.22	0.62	2.34	3.81
Ln(MIDA)	0.72	1.23	2.52	0.48	2.32	2.88

[a] The Nd and Ho data are from Table V of the present paper. The Er data are from Table IV of ref 11.

exhibit by far the greatest variations with changes in ligands, and the Ω_4 parameters show the smallest variations; (2) *relative* ligand effects on the Ω_2 parameters follow the order ODA < IDA ≈ MIDA < DPA < CDA ≈ CDO; (3) the Ω_2(complex)/Ω_2(aquo) ratios for holmium are significantly larger than those for neodymium and erbium. Turning to the experimental results given in Table XI, and considering the Ln(ODA) complexes as reference systems, we note that neodymium, holmium, and erbium complexes exhibit similar Ω_2(complex)/Ω_2(ODA) ratios, with a *slight* preferential ordering of Nd > Ho > Er.

Table VIII. Calculated Intensity Parameters for Model Structures of Nd(III) Complexes

structure	λ	calcd $\Omega_\lambda/10^{-21}$ cm^2			
		[SC][a]	[DC][a]	[SC,DC][a]	total[a]
$Nd(H_2O)_9$	2	0.1	2.9	−0.9	2.1
	4	2.6	199.2	−44.8	157.0
	6	4.4	16.2	−1.7	18.9
$Nd(H_2O)_8$	2	0	0	0	0
	4	1.0	82.5	−18.5	65.0
	6	2.0	65.7	−7.2	60.5
Nd(ODA)	2	16.3	16.3	30.1	62.7
	4	56.6	18.4	−46.9	28.1
	6	57.6	0.4	−6.1	51.9
Nd(DPA)	2	18.2	53.4	61.0	132.6
	4	58.4	28.5	−64.2	22.7
	6	56.0	0.5	−2.6	53.9
Nd(CDO)	2	15.8	59.0	59.8	134.6
	4	55.8	29.9	−69.6	16.1
	6	57.7	0.4	−0.7	57.4
Nd(CDA)	2	18.2	54.9	61.9	135.0
	4	58.4	28.6	−64.3	22.7
	6	56.0	0.5	−2.6	53.9
Nd(IDA)	2	2.2	79.2	25.5	106.9
	4	16.1	11.3	−17.7	9.7
	6	24.2	1.3	−5.2	20.3
Nd(MIDA)	2	2.0	76.3	22.6	100.9
	4	15.9	15.9	−20.9	10.9
	6	24.4	0.8	−3.5	21.7

[a] See eq 7–10 in text.

Table IX. Calculated Intensity Parameters for Model Structures of Ho(III) Complexes

structure	λ	calcd $\Omega_\lambda/10^{-21}$ cm^2			
		[SC][a]	[DC][a]	[SC,DC][a]	total[a]
$Ho(H_2O)_9$	2	<0.1	3.6	−0.6	3.0
	4	0.3	153.0	−13.3	140.0
	6	2.2	10.7	−0.9	12.0
$Ho(H_2O)_8$	2	0	0	0	0
	4	0.1	63.4	−5.5	58.0
	6	1.0	43.4	−3.7	40.7
Ho(ODA)	2	6.8	20.5	21.8	49.1
	4	16.3	14.2	−13.2	17.3
	6	28.2	0.2	−3.4	25.0
Ho(DPA)	2	7.6	67.1	44.2	118.9
	4	17.6	21.9	−20.4	19.1
	6	27.4	0.3	−1.5	26.2
Ho(CDO)	2	6.6	71.1	42.5	120.2
	4	15.8	22.5	−23.0	15.3
	6	28.2	0.3	−0.5	28.0
Ho(CDA)	2	7.6	68.9	44.9	121.4
	4	17.6	22.0	−20.4	19.2
	6	27.4	0.3	−1.5	26.2
Ho(IDA)	2	0.9	99.4	18.5	118.8
	4	3.2	8.7	−4.6	7.3
	6	11.6	0.8	−2.7	9.7
Ho(MIDA)	2	0.8	95.8	16.4	113.0
	4	3.0	12.2	−5.6	9.6
	6	11.8	0.5	−1.9	10.4

[a] See eq 7–10 in text.

The results given in Table VII show that Ω_4(Nd) > Ω_4(Ho) > Ω_4(Er) and Ω_6(Nd) > Ω_6(Ho) > Ω_6(Er) for the systems examined in this study. The Ω_6 parameters exhibit the greatest metal ion dependence, and these parameters are largest for the largest metal ion (Nd^{3+}) and smallest for the smallest metal ion (Er^{3+}) considered here. For the Ln(ODA) and Ln(DPA) complexes, the Ω_6(Nd):Ω_6(Ho):Ω_6(Er) ratios are 1.00:0.49:0.37 (for ODA) and 1.00:0.36:0.29 (for DPA). These ratios are interestingly similar to the ratios of the squares of the $\langle r^6 \rangle$ radial integrals listed in

Table X. Ratios of Calculated vs Empirical Intensity Parameters[a,b]

complex	Ω_λ(calcd)/Ω_λ(exptl)		
	λ = 2	λ = 4	λ = 6
Nd(ODA)	2.59	0.72	0.61
Nd(DPA)	2.82	0.47	0.48
Nd(CDO)	1.69	0.29	0.51
Nd(CDA)	1.93	0.32	0.44
Nd(IDA)	3.23	0.19	0.22
Nd(MIDA)	3.07	0.24	0.26
Ho(ODA)	1.27	0.43	0.59
Ho(DPA)	1.86	0.47	0.64
Ho(CDO)	1.08	0.30	0.58
Ho(CDA)	1.20	0.38	0.54
Ho(IDA)	2.90	0.15	0.23
Ho(MIDA)	2.44	0.26	0.31
Er(ODA)	0.93	1.00	0.77
Er(DPA)	1.51	1.05	0.80
Er(CDO)	1.16	0.68	0.78
Er(CDA)	1.00	0.73	0.73
Er(IDA)	2.25	0.36	0.38
Er(MIDA)	1.58	0.50	0.38

[a] Data for Nd and Ho complexes are from Tables V, VIII, and IX of the present paper. [b] Except for Er(CDO), data for the Er complexes are from ref 12.

Table XI. Relative Values of Intensity Parameters

complex	Ω_λ(complex)/Ω_λ(ODA)					
	λ = 2		λ = 4		λ = 6	
	calcd	exptl	calcd	exptl	calcd	exptl
Nd(ODA)	*1.00*	*1.00*	*1.00*	*1.00*	*1.00*	*1.00*
Nd(DPA)	2.11	1.94	0.81	1.22	1.04	1.32
Nd(CDO)	2.15	3.29	0.57	1.43	1.11	1.31
Nd(CDA)	2.15	2.89	0.81	1.81	1.04	1.43
Nd(IDA	1.70	1.37	0.35	1.30	0.39	1.09
Nd(MIDA)	1.61	1.36	0.39	1.18	0.42	0.98
Ho(ODA)	*1.00*	*1.00*	*1.00*	*1.00*	*1.00*	*1.00*
Ho(DPA)	2.42	1.65	1.10	1.00	1.05	0.97
Ho(CDO)	2.45	2.86	0.88	1.29	1.12	1.15
Ho(CDA)	2.47	2.61	1.11	1.26	1.05	1.13
Ho(IDA)	2.42	1.05	0.42	1.25	0.39	0.99
Ho(MIDA)	2.30	1.20	0.55	0.94	0.42	0.78
Er(ODA)	*1.00*	*1.00*	*1.00*	*1.00*	*1.00*	*1.00*
Er(DPA)	2.41	1.49	1.09	1.04	1.04	1.00
Er(CDO)	2.49	1.99	0.88	1.28	1.08	1.05
Er(CDA)	2.48	2.29	1.16	1.58	1.04	1.10
Er(IDA)	2.46	1.01	0.48	1.35	0.37	0.75
Er(MIDA)	2.33	1.37	0.62	1.24	0.44	0.89

Table XII. Intensity Parameters for Ln(aquo) Complexes

Ln	λ	$\Omega_\lambda/10^{-21}$ cm^2		
		exptl	calcd[a]	calcd[b]
Nd	2	9.0 ± 4.7	2.1	0
	4	45.6 ± 5.6	157.0	65.0
	6	68.8 ± 4.0	18.9	60.5
Ho	2	2.4 ± 2.3	3.0	0
	4	32.7 ± 3.4	140.0	58.0
	6	29.5 ± 1.9	12.0	40.7
Er	2	20.3 ± 2.9	3.1	0
	4	19.0 ± 3.9	133.4	55.2
	6	21.4 ± 4.4	11.3	38.4

[a] Calculated for nine-coordinate model structure. [b] Calculated for eight-coordinate model structure.

Table II: $\langle r^6\rangle^2$(Nd):$\langle r^6\rangle^2$(Ho):$\langle r^6\rangle^2$(Er) = 1.00:0.41:0.37. The metal ion dependence of the Ω_2 parameters follows the opposite order for all except the Ho(aquo) complex; that is, Ω_2(Er) > Ω_2(Ho) > Ω_2(Nd). This suggests that the Ω_2 vs the Ω_6 (and possibly the Ω_4) intensity parameters are governed by (or are derived from) different Ln–L–$h\nu$ interaction mechanisms.

Excluding the Ln(aquo) complexes from consideration, all of the complexes examined in this study contain the same charged groups (or atoms) in the inner coordination sphere. Furthermore, these charged groups (carboxylate moieties) are expected to be geometrically configured about the lanthanide ion in a similar fashion in all the complexes. The major differences between complexes are found in the chemical makeup of the (formally) uncharged donor moieties and their substituents and in the chemical compositions and geometrical dispositions of the chelate rings. As was noted earlier in this section (vide supra), only the Ω_2 parameter exhibits large variations from complex to complex for a given lanthanide ion. Whereas the Ω_6 parameter is most sensitive to the inherent electronic properties (and size) of the metal ion, the Ω_2 parameter is by far the most sensitive to structural differences in the ligand environment about the metal ion.

Model Calculations. Within the framework of our theoretical model (and excluding the Ln(aquo) complexes from consideration), our calculations show that the dynamic-coupling mechanism generally makes the dominant contributions to the Ω_2 parameters, the static-coupling mechanism makes the dominant contributions to the Ω_6 parameters, and the static- *and* dynamic-coupling mechanisms generally make comparable contributions to the Ω_4 parameters. The Ω_λ(calcd)/Ω_λ(exptl) ratios are listed in Table X. Again, note that our model calculations generally overestimate the Ω_2 values and underestimate the Ω_4 and Ω_6 values. The largest deviations between calculated and experimental values occur for the Ln(IDA) and Ln(MIDA) complexes, and these deviations are especially large for the Ω_4 and Ω_6 parameters. With respect to metal ion, the quality of agreement between calculated and experimental results follows the order Nd < Ho < Er. The calculated and experimental results show the same qualitative metal ion dependence in the Ω_4 and Ω_6 parameters, i.e., Ω_λ(Nd) > Ω_λ(Ho) > Ω_λ(Er).

The calculated results are *qualitatively* compatible with the observed ligand dependence of the Ω_2 intensity parameter; that is, Ω_2(ODA) < Ω_2(IDA) ≈ Ω_2(MIDA) < Ω_2(DPA) < Ω_2(CDA) ≈ Ω_2(CDO). This qualitative agreement (and the *lack* of quantitative agreement) is most easily seen in the results displayed in Table XI. Our calculated Ω_2 parameters are modulated primarily by the magnitude and distribution of electric dipolar polarizability in the central donor moieties of the ligands and by the $\langle r^2\rangle$ radial integrals for the 4f electrons of the lanthanide ion. Modest and physically realistic adjustments in the $\langle r^2\rangle$ and ligand polarizability parameters could be made to yield Ω_2(calcd)/Ω_2(exptl) ratios near unity for the Ln(ODA), Ln(DPA), Ln(CDO), and Ln(CDA) systems. On the other hand, small adjustments to these model parameters would not be sufficient to fix our calculated results for the Ln(IDA) and Ln(MIDA) systems. For these latter systems, it is likely that additional model structures would have to be constructed to represent adequately the principal absorbing species (complexes) in solution.

In previous work,[10,12,24] we have discussed some of the effects of (1) using different sets of lanthanide electronic parameters, $\langle r^\lambda\rangle$ and $\Xi(t,\lambda)$, (2) assigning alternative charges and polarizabilities to ligand perturber sites, and (3) changing the spatial distribution and anisotropies of ligand moiety polarizabilities. These exercises produced some interesting insights regarding the parametric sensitivity (and stability) of the intensity model. However, given the approximate nature of the model structures used to mimic the *real* complexes and the limited mechanistic basis of the intensity model, it is not particularly fruitful to pursue refinements of the types of calculations reported here. However, these calculations do provide a useful framework within which *qualitative* correlations between ligand structure, lanthanide electronic structure, and 4f–4f electric-dipole intensities may be rationalized (or at least systematized).

Hypersensitivity. Four of the absorption bands examined in this study exhibit intensities that may be characterized as "hypersensitive" to the ligand environment. These absorption bands and their underlying multiplet-to-multiplet transitions are identified in Table XIII. The data listed in Table XIII reveal significant ligand-induced enhancements of the oscillator strengths

(24) Devlin, M. T. Ph.D. Dissertation, University of Virginia, 1987.

Table XIII. Ligand Effects on the Oscillator Strengths of Hypersensitive Transitions

	f(complex)/*f*(aquo)			
complex	Nd(e)[a]	Ho(d)[b]	Er(c)[c]	Er(h)[d]
Ln(ODA)	1.29	2.79	2.08	1.88
Ln(MIDA)	1.60	3.03	2.75	2.49
Ln(IDA)	1.68	3.12	2.26	2.05
Ln(DPA)	2.00	3.86	2.95	2.65
Ln(CDA)	2.89	5.73	5.08	(4.15)[e]
Ln(CDO)	2.90	6.19	4.45	(3.58)[e]

[a] $^4I_{9/2} \rightarrow {}^4G_{5/2}, {}^2G_{7/2}$; absorption band centered near 580 nm. [b] $^5I_8 \rightarrow {}^5G_6, {}^5F_1$; absorption band centered near 450 nm. [c] $^4I_{15/2} \rightarrow {}^2H_{11/2}$; absorption band centered near 520 nm. [d] $^4I_{15/2} \rightarrow {}^4G_{11/2}$; absorption band centered near 380 nm. See ref 11. [e] Calculated from fitted oscillator strength data. See ref 11.

measured for these transitions. In addition to the *f*(complex)/*f*(aquo) ratios given in Table XIII, it is interesting to note the oscillator-strength ratios for Ln(ODA) vs Ln(DPA) vs Ln(CDA). The latter are approximately the same for the different transitions: 1.00 (ODA):1.45 (DPA):2.20 (CDA). Recall that the Ln(CDA) complexes differ from the Ln(DPA) complexes only by a 4-oxo substituent on the pyridyl ring of the central donor moiety of each ligand. However, this small difference produces a 50% increase in the intensities of the hypersensitive transitions.

The transitions making the major contributions to the hypersensitive absorption bands are as follows: $^4I_{9/2} \rightarrow {}^4G_{5/2}$, Nd(e); $^5I_8 \rightarrow {}^5G_6$, Ho(d); $^4I_{15/2} \rightarrow {}^2H_{11/2}$, Er(c); $^4I_{15/2} \rightarrow {}^4G_{11/2}$, Er(h). Each of these transitions nominally satisfies electric-quadrupole selection rules for ΔJ and ΔL, and the ΔS selection rule is also satisfied at least in part, since the $^2H_{11/2}$ and $^4G_{11/2}$ multiplets of Er^{3+} are strongly mixed in the intermediate-coupling scheme (see Table II of ref 11). According to our model calculations, the *electric-dipole* intensities of these transitions are derived primarily from correlated *dynamic couplings* between 4f–4f electric-quadrupolar transition densities and transient electric dipoles produced in polarizable ligand groups by the incident radiation field. The transition intensities depend on the strength (and symmetry) of the dynamic couplings, and the latter depend on the distribution, magnitude, and anisotropy of ligand polarizability.[13,14,17] The relative oscillator strengths listed in Table XIII for the Ln(ODA), Ln(DPA), Ln(CDA), and Ln(CDO) complexes do correlate with relative ligand polarizabilities. On the other hand, the relative oscillator strengths of the Ln(ODA), Ln(MIDA), and Ln(IDA) complexes probably reflect structural (geometrical) differences as well as differences in ligand polarizability.

The ligand-dependent intensity variations observed in the hypersensitive transitions examined in this study are quite satisfactorily accounted for by the dynamic-coupling mechanism in our intensity model. However, it is possible that other mechanisms, not included in our model, may also be important in producing these intensity variations. Recall that our model neglects all effects that might arise from f-orbital overlap with ligand orbitals (including covalency effects). It is likely that these effects will appear most prominently in the Ω_6 intensity parameters and least prominently in the Ω_2 parameters but definitive intensity calculations including orbital overlap effects have not yet been reported.

Acknowledgment. This work was supported by the National Science Foundation (NSF Grant CHE-8215815 to F.S.R.), by the National Institutes of Health (Grants DK35865 and SO7 RR05431-24 to E.M.S.), and by a grant from the Muscular Dystrophy Association (to E.M.S.).

Registry No. $Nd(ODA)_3^{3-}$, 43030-80-4; $Ho(ODA)_3^{3-}$, 58855-74-6; $Er(ODA)_3^{3-}$, 83289-78-5; $Nd(DPA)_3^{3-}$, 38721-35-6; $Ho(DPA)_3^{3-}$, 38785-79-4; $Er(DPA)_3^{3-}$, 38682-38-1; $Nd(CDO)_3^{6-}$, 113474-75-2; $Ho(CDO)_3^{6-}$, 113474-74-1; $Er(CDO)_3^{6-}$, 107454-34-2; $Nd(CDA)_3^{6-}$, 113474-77-4; $Ho(CDA)_3^{6-}$, 113474-76-3; $Er(CDA)_3^{6-}$, 107454-33-1; $Nd(IDA)_3^{3-}$, 12561-55-6; $Ho(IDA)_3^{3-}$, 83233-72-1; $Er(IDA)_3^{3-}$, 83289-79-6; $Nd(MIDA)_3^{3-}$, 89746-87-2; $Ho(MIDA)_3^{3-}$, 83233-73-2; $Er(MIDA)_3^{3-}$, 83248-18-4; $Nd(H_2O)_9^{3+}$, 54375-24-5; $Ho(H_2O)_9^{3+}$, 55664-37-4; $Er(H_2O)_9^{3+}$, 56422-25-4; $Nd(H_2O)_8^{3+}$, 62006-59-1; $Ho(H_2O)_8^{3+}$, 63213-08-1; $Er(H_2O)_8^{3+}$, 63118-71-8; Nd^{3+}, 14913-52-1; Ho^{3+}, 22541-22-6; Er^{3+}, 18472-30-5.

Contribution from the Department of Chemistry, University of Missouri—Rolla, Rolla, Missouri 65401, Department of Physics, University of Liverpool, Liverpool L69 3BX, England, Institut de Physique, Universite de Liège, B-4000 Sart-Tilman, Belgium, and Dipartimento di Chimica Inorganica, Metallorganica ed Analitica, Universita di Padova, Via Loredan, 4, I-35131 Padova, Italy

Mössbauer Effect Study of $Fe_3(CO)_{12}$

Fernande Grandjean, Gary J. Long,* Christopher G. Benson, and Umberto Russo

Received September 22, 1987

The Mössbauer effect spectrum of $Fe_3(CO)_{12}$ has been measured from 4.2 to 295 K, and the results, when analyzed in terms of the two expected quadrupole doublets, reveal an unusual temperature dependence, first in the quadrupole interaction for the unique nonbridged iron site, second in the relative area of the two components of the quadrupole doublet associated with the two chemically equivalent carbonyl-bridged iron sites, and third in the relative area of these two quadrupole doublets. The first of these may be understood in terms of a negative quadrupole interaction for the unique iron site, produced principally by a negative, temperature-dependent, valence contribution to the electric field gradient. The second results from the large vibrational anisotropy associated with the bridged iron sites, which leads to the Goldanskii–Karyagin effect and an asymmetric doublet. An analysis based on the single-crystal thermal ellipsoid anisotropy of the bridged iron sites is successful in explaining the observed asymmetry. The third results from the different temperature dependence of the recoil-free fractions observed for the two chemically quite dissimilar iron sites.

Introduction

The determination of the solid-state structure of triiron dodecacarbonyl, $Fe_3(CO)_{12}$ (I), a 50-year story, was nicely summarized by Desiderato and Dobson.[1] Its single-crystal structure was solved by Wei and Dahl[2] and further refined by Cotton and Troup.[3] The molecule has C_{2v} symmetry as shown in Figure 1 and has one unique iron atom, Fe_1 or Fe_A, bonded to four terminal

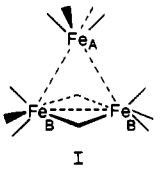

I

carbonyl ligands and two chemically equivalent iron atoms, Fe_2 and Fe_3 or Fe_B, bonded to three terminal carbonyl and two

* To whom correspondence should be addressed at the University of Missouri—Rolla.

(1) Desiderato, R., Jr.; Dobson, G. R. *J. Chem. Educ.* **1982**, *59*, 752–756.

0020-1669/88/1327-1524$01.50/0